Figure S1

A Paddle experiment

$\theta = \pi$ excursion $\theta = 0$

return

walking arena
$\theta = \dfrac{\pi}{2}$

B Reverse paddle control experiment

$\theta = \dfrac{\pi}{2}$

return
excursion

$\theta = 0$ $\theta = \pi$

walking arena

C Average velocity in response to forward or reverse paddle motion

— Reverse paddle
— Forward paddle

Canton S

velocity (mm/sec)

Time(secs)

D Forwards paddle

velocity (mm/sec)

***   ***

3s BEFORE   DURING   3s AFTER

E Reverse paddle

velocity (mm/sec)

***   ***

3s BEFORE   DURING   3s AFTER

Figure S2

Figure S3

A — Single flies (n=99 flies); Cohorts of ten flies (n=800 flies); Shadow event. Fraction of flies off food vs Time in frames (33Hz). *Canton S*

B — Flies off food, raster plot (single flies, n=99 flies). Individual trials vs Time in frames (33Hz).

B' — Boxed region from B. Individual trials vs Time in frames (33Hz).

C — Shadow-induced dispersal exhibits scalability with swipe number. Fraction of flies off food vs Time in frames (33Hz). Cohorts of ten flies (n=800 flies); Single flies (n=99 flies); Shadow event.

D — Shadow-induced dispersal exhibits scalability with swipe number. Fraction of flies on food patch. baseline, 10 fly; post-pass 1, 10 fly; post-pass 2, 10 fly. ***

E — Cooperative suppression of flight. Fraction of flies on food patch. baseline, 1 fly; baseline, 10 fly; post-pass 2, 1 fly; post-pass 2, 10 fly. ***

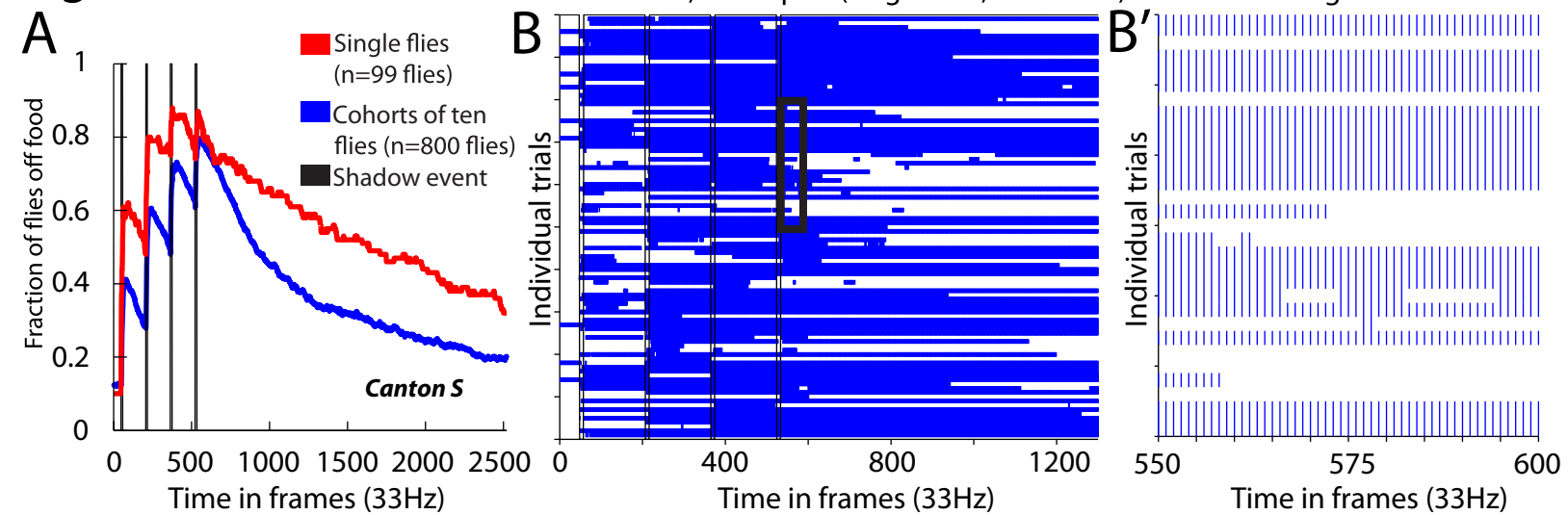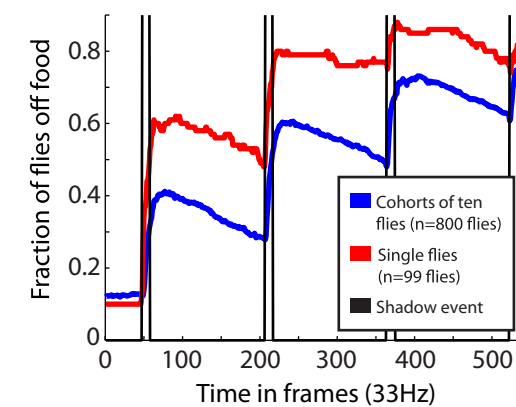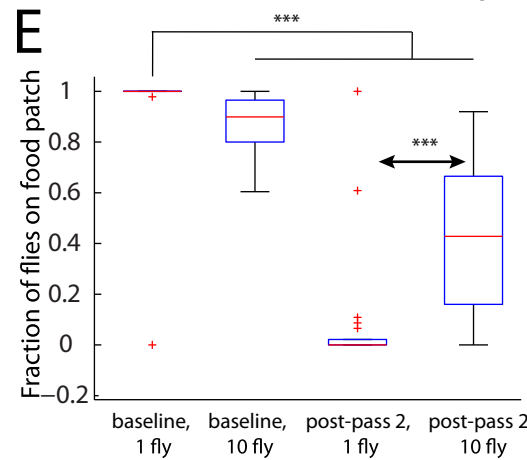**F** — Sensitization of dispersal from food in 10-fly cohorts. Fraction of flies on the food prior to swipe that leave the food. Shadow pass 1, 10 fly; Shadow pass 2, 10 fly. ***

G — Cooperative return kinetics. Fraction of flies off food vs Time in frames (33Hz). Cohorts of ten flies (n=800 flies); Single fly experiments (n=99 flies); Exponential fit, single fly expt; (dashed) Exponential fit, 10 fly expt.
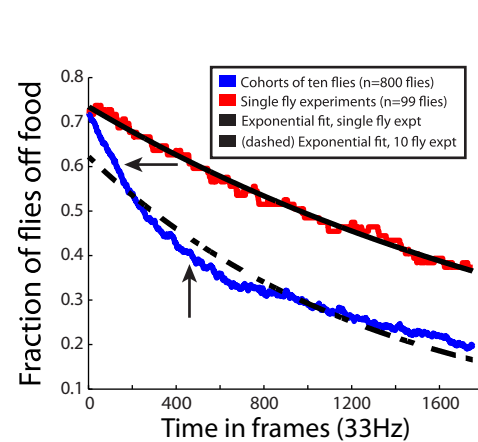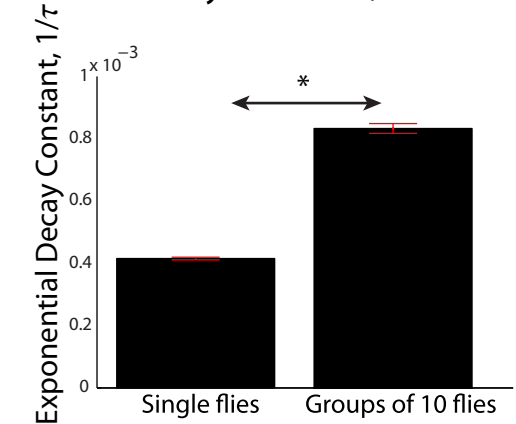
H — Decay constant, $1/\tau$. Exponential Decay Constant, $1/\tau$. Single flies; Groups of 10 flies. *

I — Flies off food; Flies on food. velocity (mm/s) vs time (frames).

J — Flies off food; Flies on food. linear fit to peak velocity vs pass number, p. BL. SLOPE: on, off. *

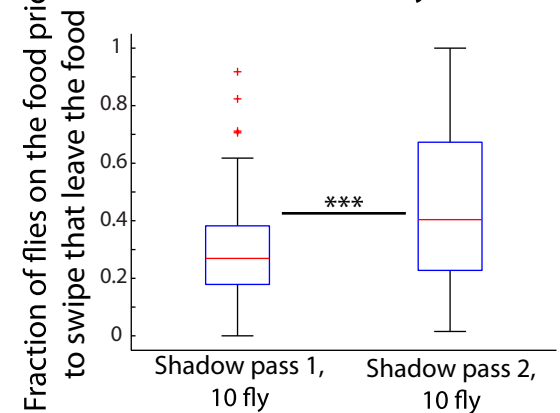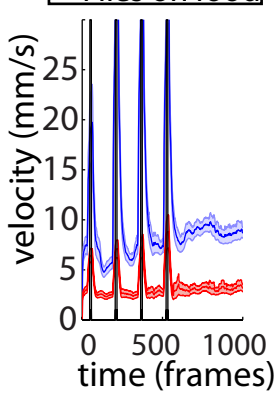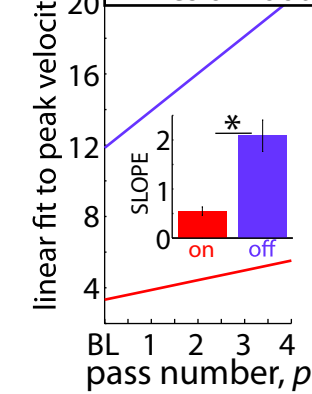**K** — BL = baseline; PS = post-shadows (1s); on = on food; off = off food. peak velocity (mm/s). BL (on); PS (on); BL (off); PS (off). ***
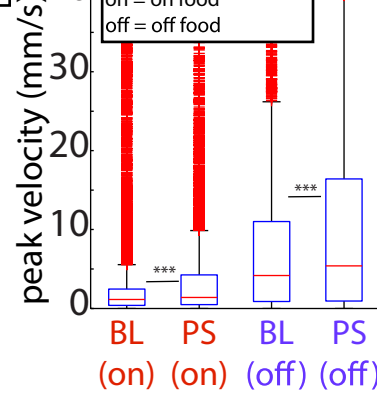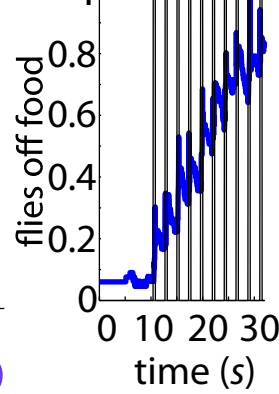
L — flies off food vs time (s).

M — Fraction of flies (n=62) leaving food after first shadow. leaving; not leaving.

Figure S4

Group-level habituation experiments on food (panels A-C)

A

Shadows begin
(ISI = 10 seconds)

Loading onto food

Shadow-induced avoidance

Flies habituated to the shadow stimulus

Fraction of flies off food patch

Time, in seconds

B

$$LI = \frac{nFlies_{before} - nFlies_{after}}{nFlies_{before}}$$

Leaving Index, LI (+/- sem)

Pass number

C

Leaving Index, LI

***

Passes 1-30   Passes 31-60
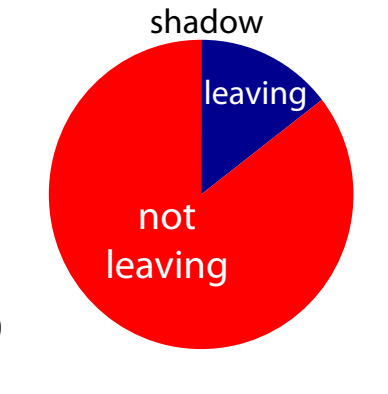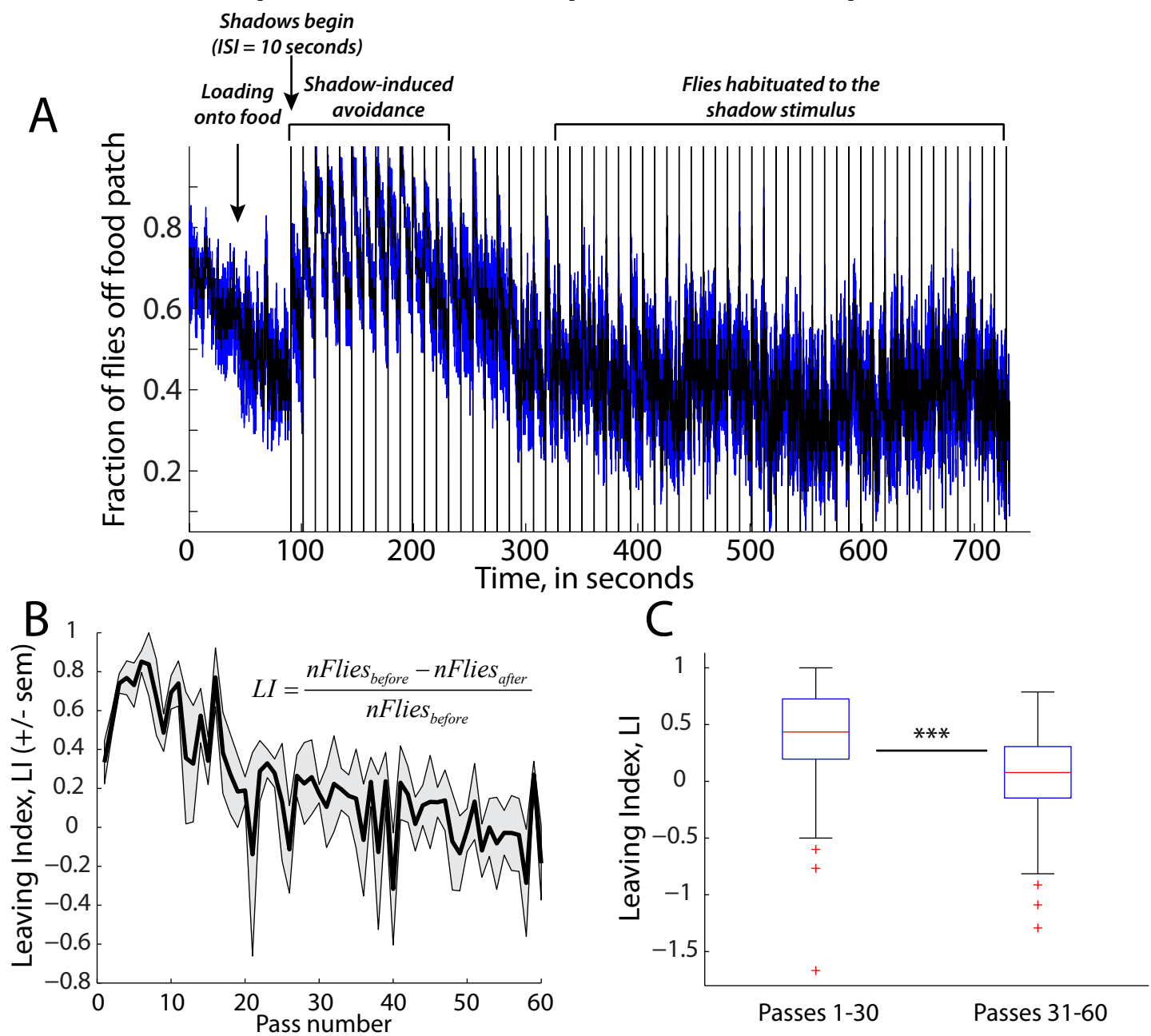
Single fly integration experiments in the absence of food (panels D-F)

D

single fly setup

$\theta = \pi$

excursion
return

$\theta = 0$

walking arena

$\theta = \frac{\pi}{2}$

E

Peak velocity (mm/s)

***   ***

BL   10p   BL   10p
      ISI=1s   ISI=10s

F

Peak hopping fraction

***   ***

BL   10p   BL   10p
      ISI=1s   ISI=10s

Figure S5

A Excursion pass

B Dwell time, **DT** (**pause**)

C Return pass

D Dispersion metric, m

$$m = \sum_{i=1}^{5} k_i \cdot d_i \quad k_i = \begin{cases} 1, \text{ if fly } i \text{ is off food} \\ 0, \text{ otherwise} \end{cases}$$

E

- return pass
- excursion pass

m

DT (sec)

F

$m_{return} - m_{excursion}$

DT (sec)

G

$m_{return} - m_{excursion}$

DT (sec)

**

Figure S6

A

Half-paddle experiment (no food present)

$\theta = \pi$ $\theta = 0$

excursion
return

control arena

walking arena

$\theta = \dfrac{\pi}{2}$

B

Mean fraction of flies in the shadowed area

- before shadows
- during shadows
- after shadows

fraction of flies

shadowed area

***   *   ***

***   ***

Full paddle experiments   Half paddle experiments

C

Time series: Half paddle versus full paddle

fraction standing in shadowed area

Time(secs)

— Full paddle experiment
— Half paddle experiment
||||| Shadow sweeps
---- Expected fraction
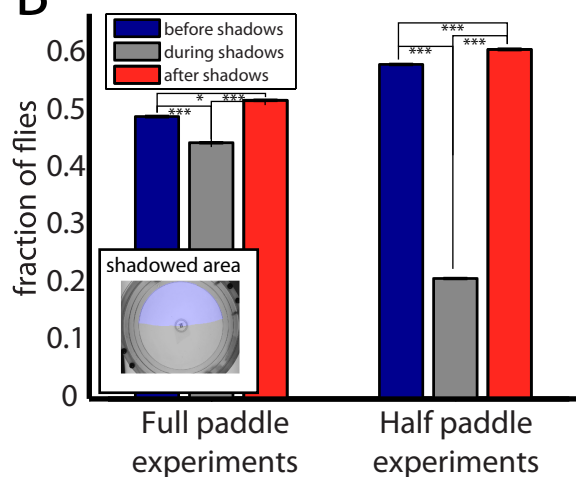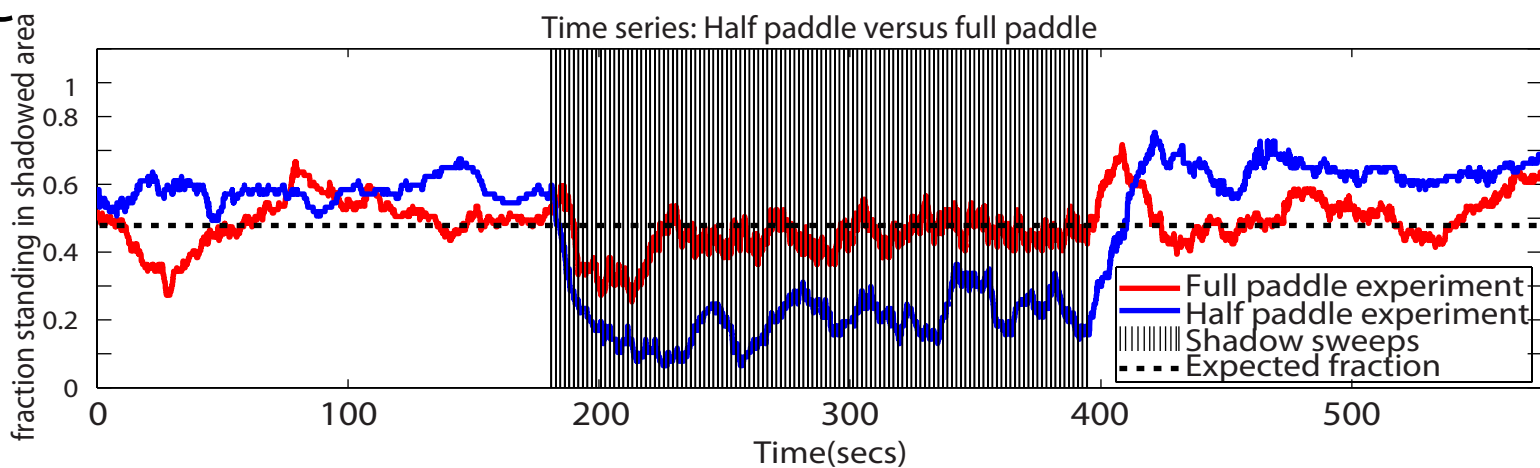
D

Food-based experiment (single fly)

initial condition (feeding)

swipe-induced dispersion from food
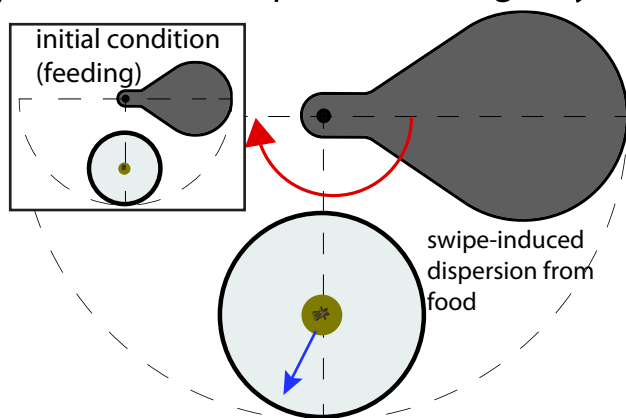
E

Trajectories due to pass 1
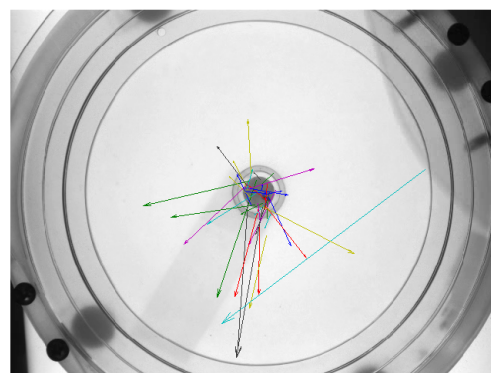
F

Trajectories due to pass 1 (centered)
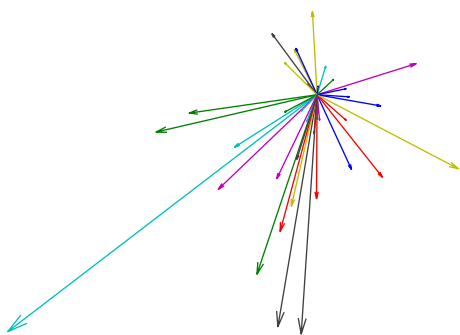
G

Components deviate from zero (away from moving paddle)

Trajectory component

*   **

Horizontal   Vertical

Figure S7

A Freezing (> 1s)

Single fly trials

← *shadow passes (ISI=15s)*

Time (s)

B Hopping

Single fly trials

Time (s)

C Freezing and Hopping

Single fly trials

Time (s)

D Fraction of flies freezing (> 1s)

← *shadow passes (ISI=15s)*

Time (s)

E Fraction of flies hopping

Time (s)

F Fraction freezing, hopping

Time (s)

G Cross correlation (shadow with freezing > 1s)

95% confidence interval

Time (s) relative to shadow pass

H Cross correlation (shadow with hopping)

Time (s) relative to shadow pass

I Cross correlation (hopping with freezing)

Time (s) relative to hopping event

J Fraction of flies freezing (> 1s)

*** **

*** **

** **

baseline   *post-pass 1*   *post-pass 2*

K Fraction of flies hopping

*** **

*** **

baseline   *post-pass 1*   *post-pass 2*

Supplemental figure legends

Figure S1: The structures supporting the paddle motor are mechanically isolated from the structure supporting the flies' covered arena by using separate support systems. This control experiment shows that any hypothetically uncontrolled vibration is unable to make the flies respond to paddle motion when it is not visible to the flies. **(A)** The experimental excursion and return paradigm. **(B)** The control paradigm, in which the paddle executes excursions and returns such that it does not pass over the arena. It is invisible to the animals in this case. **(C)** A time series showing, respectively, forward paddle experiments (*blue* envelope) and backward paddle experiments (*red* envelope). **(D)** Population level velocity before, during, and after the excursion and return passes under the experimental paradigm. Velocity increases during shadowing, and remains elevated (***). **(E)** Population level velocity before, during, and after excursion and return passes under the control pa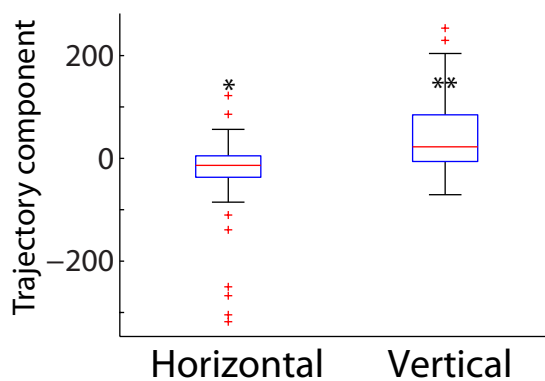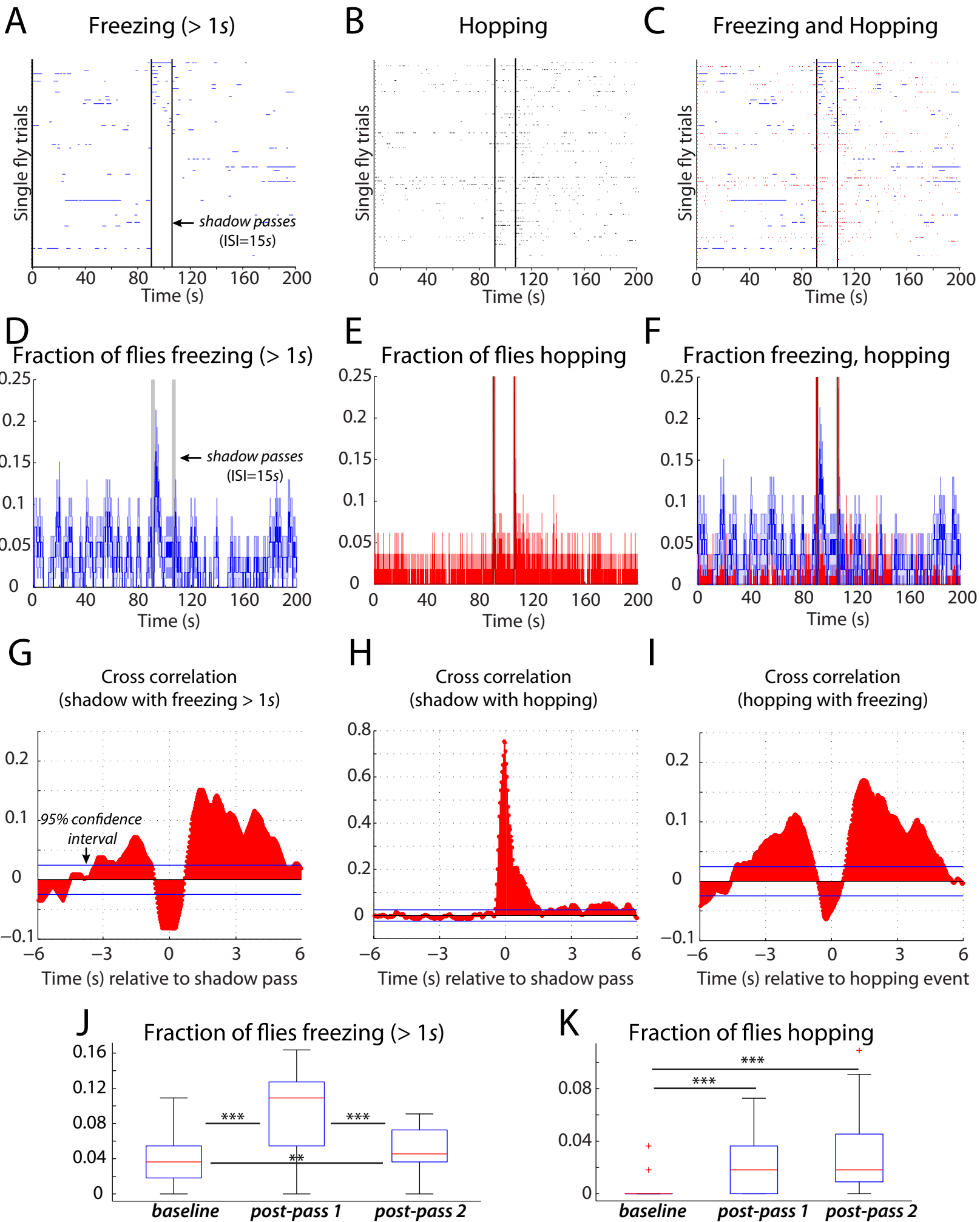radigm. Note that overall velocity tends to decrease with time (***). Sample sizes in panels C-E are $n=120$ flies for the forward paddle and $n=120$ flies for the reverse paddle. Figure S1 relates to Figure 1.

Figure S2: Supplemental figure demonstrating scalability as a function of pass number p, both for peak velocity, and for hopping, when ISI=1s but not ISI=3s. **(A)** Peak velocity, normalized to baseline, for $p=0…$ 10 with ISI=1s. There is an increasing trend (multiple significant pair-wise differences). **(B)** Peak velocity, normalized to baseline, for flies receiving 0…10 passes with ISI=3s. None of the values are different from each other from $p=2$ to 10 passes (Kruskal-Wallis test); scalability is lost. **(C)** Pair-wise tests confirm a monotone increase in hopping frequency when ISI=1s (*). **(D)** The trend disappears when ISI=3s. **(E)** Hopping frequency is different from baseline when ISI=1s, both for $p=2$, and for $p=10$ (multiple significant pair-wise differences). Moreover, $p=2$ differs from $p=10$, demonstrating scalability. **(F)** Hopping frequency differs from baseline for both the $p=2$ and $p=10$ when ISI=3s (**). However, there is no difference for $p=2$ versus $p=10$. In the ISI=1s, for the $p=0…10$, experiments, sample sizes are, respectively, 220, 110, 109, 108, 120, and 119 flies. For ISI=3, for $p=0…10$ experiments, sample sizes are, respectively, 220, 100, 110, 100, 110, and 118 flies. Cohort sizes were ~10 flies each. Stars indicate statistical significance. Panels in Figure S2 use same datasets as Figure 3. Figure S2 relates to Figure 3.

Figure S3: (A) Fraction of flies off food versus time, for single flies (*red*) and cohorts of flies (*blue*), during shadow passes (*black bars*). **(B)** Raster plot for single flies off food (*blue*), with shadow passes (*black*). **(B')** Closeup of the boxed region. **(C)** Scalable escape kinetics for single flies (*red*) and cohorts of flies (*blue*). **(D)** Fraction of flies off food versus pass number p, which declines with p (***). **(E)** Fraction of flies leaving the food is suppressed in cohorts (***). **(F)** Evidence for sensitization in cohorts. A greater proportion leave after pass 2 versus pass 1 (***). **(G)** Cooperative group-level return kinetics, based on decay constants **(H)**. **(H)** Decay constants are different (*,see bottom of legend). **(I)**Flies on food (*red*) react with lower locomotor activity than flies off food (*blue*). **(J)** Linear fits to the peak velocity in the 1s following each shadow pass for flies on food (*red*) and off food (*blue*). Slopes are significantly different (*; see bottom of legend). **(K)** Baseline and post-shadow velocities for on food and off food

flies(***). **(L-M)** Flies in some experiments ignore first shadow pass. Ten fly data from Figure 6C is repeated in panels A-B. Sample sizes in **(A-H)** are *n*=99 flies (99 experiments); and *n*=810 flies (81 experiments). Sample size for panels **(K-L)** was 62 flies initially on food (of 67 total). Decay constants in **(H)** and **(J)** differ (*) because their 95% CI's do not overlap. Figure S3 relates to Figures 6-7.

Figure S4: (A-C) On long timescales with a long ISI, flies can habituate to the shadow paddle while feeding on a central food resource. **(A)** A time series demonstrating the habituation process. The vertical axis shows the fraction of flies off the food patch. Vertical bars (*black*) represent shadow passes (ISI=10*s*). Prior to the first shadow arrival, the fraction of flies off food decreases as flies are loading onto the food patch. Upon the arrival of the first shadow, flies are dispersed from the food resource, and continually re-approach the food, but are repeatedly dispersed by oncoming shadows. As the flies begin to habituate, they show less and less reaction to the shadow. **(B)** A leaving index to quantify the habituation process, which is computed for each shadow pass. The metric is the fraction of flies on the food prior to the pass that leaves in response to the shadow. It can be negative if more flies come back than were dispersed for a given shadow pass. Error bars represent SEM envelopes. **(C)** The first 30 and last 30 shadows have statistically significantly different leaving indices (***). **(D-F)** A demonstration of leaky integration in single flies in an assay without food for ISI values of 1s and 10s. Flies were given 90 seconds to acclimate to the chamber, and then received 10 passes of the shadow, with an ISI value of either 1 second or 10 seconds. Peak velocity **(E)** and hopping frequency **(F)** both show statistically significant increases (***, see bottom of legend) relative to baseline for the 1 second ISI, but not for the 10 second ISI. Hence, in addition to showing scalability (Figure 5), single flies exhibit leaky integration. Sample sizes for panels **(A-C)** are *n*=40 flies (4 cohorts of 10 flies each).   Sample sizes for panels **(D-F)** were 26 flies for ISI=10 and 27 flies for ISI = 1. All pair-wise tests are corrected for multiple comparisons. Figures S4A-C relate to Figures 6-7; Figures S4D-F relate to Figure 5.

Figure S5: Shorter dwell times lead to greater dispersion of the flies from a food resource *for a single excursion and return of the paddle*, consistent with the existence of a labile internal variable that accumulates following each pass, and hence, leaky integration. **(A)** The excursion pass. **(B)** The dwell time (DT, *green*), or pause between the excursion pass and return pass. **(C)** The return pass. **(D)** A metric of dispersion. "*m*" is computed as the sum of the distances of all flies that are off the food from the food. **(E)** The *m* values for the return and excursion stimuli (+/- SEM envelopes). Each data point represents three trials on the same cohort of five flies feeding on the food resource (one cohort per DT value). **(F)** Difference between the *m* value in the return pass and in the excursion pass (delta m), versus DT value. If shadow stimuli are summated and the first shadow is sub-threshold for significant fly dispersal, we should expect that longer DT values lead to smaller delta m values. Trend is different from a flat line (**;

Kruskal-Wallis test). **(G)** Grouping DT values (30s and 20s in the first group; 10s and 5s in the second; and 0-2s in the third), we find a statistically significant difference between the longest DT values and the shortest DT values, and a trend in the medians, consistent with leaky integration at the group level (**multiple significant pair-wise differences, see bottom of legend). Sample sizes for panels **(D-F)** were 5 flies per DT condition, with each cohort used in three separate trials. All pairwise tests are corrected for multiple comparisons. Figure S5 relates to Figures 6-7.

Figure S6: Supplemental figure to provide supporting evidence that the shadow is an aversive stimulus. When the shadow is presented asymmetrically **(A)**, flies tend to avoid **(B-C)** the shadowed region **(B, *inset*)**. **(D-G)** Flies on food tend to escape from the food in a direction that correlates with the direction of shadow motion, suggesting that flies orient to avoid collision with the moving paddle. The horizontal component of the median trajectory is negative (points to the left) and the vertical component is positive (positive points downwards in this example). Both components are statistically significantly different (*,**, see bottom of legend) from zero **(G),** consistent with a path of paddle avoidance. Sample sizes for panels **(A-C)** are 80 flies for the half paddle experiment and 100 flies for the full paddle. The sample size for panels **(D-G)** was *n*=40 flies. See also Movie S6. Asterisks directly above box plots represent statistical significance with respect to the zero value. Figure S6 relates to Figures 1-3 and 5-7.

Figure S7: (A) A raster plot of freezing (*blue*; taking a minimum freezing duration of 1 second) in single flies based on a single excursion and return of the paddle (ISI=15s). Runs were sorted according to the number of freezing events between the shadows. Heterogeneity is apparent, with some flies never freezing, some freezing after the shadows, and others being inactive even in the baseline condition. **(B)** A raster plot of hopping (*black*), with the same ordering as in **(A)**. Hopping is heterogeneous, with some flies hopping at baseline, and others never hopping. There is a clear enrichment following stimulus delivery. **(C)** An overlay of the freezing (*blue*) and hopping (*red*) raster plots. **(D)** A time series of the fraction of flies freezing (≥1s). **(E)** A time series of the hopping fraction. **(F)** An overlay of the two time series. **(G)** Cross correlation between the shadow's presence and freezing (>1s). Values outside of the blue 95% confidence intervals are statistically significant. **(H)** Cross correlation between the shadow and hopping. **(I)** Cross correlation between freezing and hopping. **(J)** Freezing (>1s) is enriched following the shadows, relative to baseline (see bottom of legend). **(K)** Hopping is enriched following the shadows (see bottom of legend), relative to baseline. Figure S7 relates to Figure 5.

Supplemental experimental procedures

Contents

(1.1) Mathematical model of a leaky integrator: We modeled shadow integration in terms of a small reservoir whose water content is analogous to the total shadow integral (Figure 4A). Shadows, when present, add water to the reservoir. Meanwhile, a hole in the reservoir's base creates a slow leak in the water content. Closely spaced shadow sequences fill the reservoir at a rapid rate (thus minimizing inter-shadow leakage), whereas more widely spaced shadow sequences fill it gradually and with greater inter-shadow leakage. Intuitively, for a given shadow sequence, the relative strengths of the fill rate and the leak rate are expected to lead to qualitatively different dynamics in the water level. In this section, we derive expressions for the water level in the reservoir as a function of the set of shadow times.

To derive a model describing the integrated value of x (the level of the reservoir) as a function of time (t), it is first necessary to write down the differential equation that describes the rate of change of the water level in the reservoir. This equation is based on two assumptions:

(1) Each shadow adds a constant value, κ (e.g., units of ml), to the reservoir level (x); and

(2) the reservoir level decays with time at a rate proportional to its magnitude at a given time ($x(t)$).

When T_S^i is the time, in seconds, at which the ith shadow of a series of n shadows occurs, the above assumptions yield the following differential equation:

$$\frac{dx}{dt} = \kappa \left[\sum_{i=1}^{n} \delta \left(t - T_S^i \right) \right] - \alpha \cdot x(t) \qquad \text{(S1)},$$

where α is the decay constant, and κ is the amount of water added by each shadow.

Note: Readers from technical fields (eg. engineering) may wish to skip directly from equation S1 to equation S9.

Before examining S1 in detail, it is instructive to consider a simplified version. Suppose there is no leakage, and there is only a single shadow in the entire shadow series. For this case, equation (S1) would be the following, where T_S^1 is the time of the single shadow's arrival:

$$\frac{dx}{dt} = \kappa \delta \left(t - T_S^1 \right) \qquad \text{(S2)}.$$

Since no water is added at times when $t \neq T_S^1$, it is necessary to use a **delta function** (δ in the above equations), which is flat and equals zero everywhere except when its own argument is zero. At this single point, the delta function creates a very thin peak of infinite height (which integrates to 1). Hence, in equation S2, the delta function $\delta \left(t - T_S^1 \right)$ makes $dx/dt = 0$ at all time points except when $t = T_S^1$, where it has an infinite peak. The integral of equation S2 (assuming the reservoir is empty to start with), is written in terms of the Heaviside function, H, which equals zero when its argument is <0, and equals one when its argument is ≥0. Hence, the solution to S2 is:

$$x(t) = \kappa H\left(t - T_S^1\right) \tag{S3},$$

which equals zero prior to $t = T_S^1$, and equals κ forever after, consistent with a single cup of

water of volume κ being poured into the reservoir at time $t = T_S^1$.

If instead of a single shadow, there were two shadow times T_S^1 and T_S^2, then the equation S2

would be:

$$\frac{dx}{dt} = \kappa\delta\left(t - T_S^1\right) + \kappa\delta\left(t - T_S^2\right) \tag{S4}.$$

If the reservoir is initially empty, integrating the above equation yields two steps in x's value: a

first step at which x increased from 0 to κ at time t=T_S^1, and a second step at which x increased

from κ to 2 κ at time T_S^2. The expression is given by the following:

$$x(t) = \kappa H\left(t - T_S^1\right) + \kappa H\left(t - T_S^2\right) \tag{S5}$$

which is in terms of a sum of two Heaviside functions, each of which corresponds to a delivered

shadow. If there were n shadows instead of only 2, equation S4 would be:

$$\frac{dx}{dt} = \kappa\delta\left(t - T_S^1\right) + \kappa\delta\left(t - T_S^2\right) + \ldots + \kappa\delta\left(t - T_S^n\right) \tag{S6}.$$

For this case, for an initially empty reservoir, the integral is:

$$x(t) = \kappa H\left(t - T_S^1\right) + \kappa H\left(t - T_S^2\right) + \ldots + \kappa H\left(t - T_S^n\right) \tag{S7}.$$

which produces a curve that looks like stair steps, with a step in the *x* value of size κ occurring

at each shadow value. Re-writing equation (S7) in terms of sigma notation, we have the right

hand side of equation S1 in the absence of leakage:

$$\frac{dx}{dt} = \kappa \left[\sum_{i=1}^{n} \delta\left(t - T_S^i\right) \right] \tag{S8}.$$

In the case where the reservoir leaks at a rate proportional to *x* scaled by a constant α (sec^{-1}), it

is necessary to add a second term (e.g., *x* ml lost per second). The leak rate is negative because

it decreases the amount of water at a rate proportional to the amount of water present, *x(t)* at

time *t,* and is therefore equal to $-\alpha \cdot x(t)$ (ml/sec, in this example set of units). Adding the leak

rate to equation S8 gives us the full equation (S1).

To compute the cumulative value of *x* over time given by equation (S1), it is necessary to solve

the equation. If the reservoir is empty to start with, the solution for (S1) is the following:

$$x(t) = \sum_{i=1}^{n} \kappa e^{-\alpha\left(t - T_S^i\right)} H\left(t - T_S^i\right) \tag{S9}$$

A sample plot representing this equation is provided in Fig. 4B. This equation shows how the

discrete peaks of water addition, together with the leak of water between times of water

addition, yield a cumulative (integrated) value of *x* over time. Note that taking the derivative

with respect to time of equation (S9) does not yield the exact expression observed in equation

S1. The derivative of S9 is the following:

$$\frac{dx}{dt} = \kappa e^{-\alpha\left(t - T_S^i\right)} \sum_{i=1}^{n} \delta\left(t - T_S^i\right) - \alpha \cdot x(t) \tag{S10}$$

Close inspection of the exponential factor shows that it can be neglected, because it equals one when shadows are present (and so doesn't affect the value of the delta function). Conversely, when shadows are absent, it is multiplied by the delta function, which equals zero. Hence, the exponential factor is not needed.

Note: Readers from technical fields (eg. engineering) may wish to skip directly to equation S14 under the section entitled, "*Scaled (dimensionless) version of model.*"

To understand equation S9 (the solution to S1 when the reservoir is empty to start with), consider the simplest case where only 1 shadow is delivered. In that case, the value of x is given by:

$$x(t) = \kappa e^{-\alpha\left(t-T_S^1\right)} H\left(t-T_S^1\right) \tag{S11}.$$

This equation equals zero at times before the shadow is delivered ($t < T_S^1$), and equals κ (eg. mL) at the moment of shadow delivery, $t = T_S^1$. At all subsequent times, equation S11 describes the decay in x, given by $x(t) = \kappa e^{-\alpha\left(t-T_S^1\right)}$, because the Heaviside function $H\left(t-T_S^1\right)$ changes its value from zero to one at time $t = T_S^1$.

Now consider a case where two successive amounts of $x = \kappa$ are delivered, at time $t = T_S^1$ and $t = T_S^2$. In that case the equation describing $x(t)$ is given by:

$$x(t) = \kappa e^{-\alpha\left(t-T_S^1\right)} H\left(t-T_S^1\right) + \kappa e^{-\alpha\left(t-T_S^2\right)} H\left(t-T_S^2\right) \tag{S12}$$

First, suppose that the shadows are effectively very far apart, ie $T_S^2 \gg T_S^1$ and/or the leak rate is

very rapid. In this scenario, when $t > T_S^2$, the first term in the above equation is negligible

because the exponential from the first term has severely decayed, and equation S10 effectively

becomes $x(t) \approx \kappa e^{-\alpha(t - T_S^2)} H(t - T_S^2)$. However, if the time between successive shadows T_S^1 and

T_S^2 is sufficiently short and/or the decay rate is sufficiently slow so that residual water from the

first shadow remains, then the first term cannot be neglected, and x(t) at times $t > T_S^2$ will be a

combination of the amount of x left over from the first shadow, plus the additional amount of x

= κ delivered at $t = T_S^2$.

For multiple (n) shadows, the general form of the integrated value of x(t) is:

$$x(t) = \kappa e^{-\alpha(t - T_S^1)} H(t - T_S^1) + \kappa e^{-\alpha(t - T_S^2)} H(t - T_S^2) + \ldots + \kappa e^{-\alpha(t - T_S^n)} H(t - T_S^n) \qquad \text{(S13).}$$

This equation is the expanded form of that given in (S9).

Scaled (dimensionless) version of model

The above models can be used to generate curves for x(t) from arbitrary combinations of the

parameters, α, κ, the number of shadows, n, and the ISI (which is $T_S^{i+1} - T_S^i$ for a set of regularly

spaced shadows). However, comparing the behavior of the model under different

combinations of parameter values, when there are 4 parameters, can be cumbersome. In order

to facilitate such comparisons, and therefore better illustrate how the model behaves under

different conditions, it is useful to develop a form of the model with fewer free parameters.

We note that due to the form of equation S1, the value of κ is actually irrelevant to the shape of the solution (it simply scales the y-dimension). We can define a scaled, "dimensionless" new variable, ξ, which is the ratio of x and κ:

$$\xi = \frac{x}{\kappa} \qquad (S14).$$

Since x and κ each have the same units (e.g., milliters), the new variable ξ is dimensionless, i.e., has no units. Therefore it essentially normalizes values of x for regimes with different κ's and re-scales the y-axis. Analogously, we re-define the time axis (x-axis) in terms of the leak rate, which has units of sec^{-1}:

$$\tau = \alpha \cdot t \qquad (S15).$$

Using these dimensionless variables, we can now re-write the differential equation (S1) as:

$$\frac{d\xi}{d\tau} = \left[\sum_{i=1}^{n} \delta\left(\tau - \tau_S^i\right) \right] - \xi(\tau) \qquad (S16).$$

and the corresponding solution (when the reservoir is empty to start with) to this equation as:

$$\xi(\tau) = \sum_{i=1}^{n} e^{-\left(\tau - \tau_S^i\right)} H\left(\tau - \tau_S^i\right) \qquad (S17).$$

Figure 4B' illustrates model output for the re-scaled model (equation S17). For comparing different regimes with regularly spaced shadows, this model now has effectively two free parameters: the ISI value and the total number of shadows n. Using this minimal set of parameters, we can more easily illustrate the behavior of the model over the space of its

solutions in a graphical manner (eg, see Figures 4J, K). As above, note that taking the derivative of equation S17 yields an expression like S16, but with an exponential term out front:

$$\frac{d\xi}{d\tau} = \left[\sum_{i=1}^{n} e^{\left(\tau - \tau_S^i\right)} \delta\left(\tau - \tau_S^i\right) \right] - \xi\left(\tau\right) \qquad \text{(S18)}.$$

The exponential can be ignored, because it is multiplied by the delta function, which is zero except when shadows occur (at which point the exponential equals 1).

(1.2) Technical definitions of persistence and scalability: For quantification of persistence and scalability in the mathematical model (see Figures 4I-K), we defined "scalability," to be the distance between the trough following the first shadow, and the trough preceding the last shadow (Figure 4I). As a function of diverse pass numbers and ISI's, we find that in general, scalability increases with pass number and rapidly decreases with increasing ISI (Figure 4J). Peak height similarly increases with pass number and decreases with ISI (Figure 4K).